SLAC-PUB-12201
revised Jan. 2007

Comparison of EGS5 simulations with experiment

W. Ralph Nelson and Clive Field *

Stanford Linear Accelerator Center, Stanford University, Stanford, CA 94309, U.S.A.

Abstract

Simulations, made using EGS5, of the longitudinal and radial distributions of energy deposition of electrons of various energies are compared with experimental results in the literature. Energies and materials are: 1 GeV in water and aluminum; 6 GeV in aluminum, copper and lead; and (longitudinal only) 28.5 GeV in alumina (Al_2O_3). There is general agreement within a few percent over most of the shower profile. Substantial discrepancies are noted at depths far beyond shower maximum, reaching ∼30 - 50% in the cases of lead and copper at 6 GeV. .

Key words: electromagnetic shower, benchmark, simulation
PACS: 02.70.Uu, 29.40.Vj

Submitted to Nuclear Instruments and Methods in Physics Research A

* Corresponding author. Tel.: + 1-650-926-2694; fax: +1-650-926-4178
Email address: sargon@slac.stanford.edu (Clive Field).

Work supported by the US Department of Energy contract DE-AC02-76SF00515

1 Introduction

Knowledge of the lateral and longitudinal distributions of energy deposition in electromagnetic cascades is important for event reconstruction in experiments using high energy particles. Devices for recording these cascades, or showers, are in use in the fields of particle physics, nuclear physics and cosmic ray physics. Many types of equipment, often referred to as calorimeters, have been used for this purpose, and their performance generally must be studied, either to optimize design or for calibration, using shower simulation codes.

Among the numerous programs available today for performing Monte Carlo studies of electromagnetic showers, the EGS code system [1] was the first in widespread use in high energy physics. It has been used as a reference model for codes that were to follow [2]. The authors of Geant4 [3], nowadays the most popular code used in the high energy physics community, have used EGS4 as a benchmark for their electron-positron-photon transport [4]. EGS4 has also been used in such simulation code systems as LAHET [5], GHEISHA [6], CALOR [7] and HERMES [8]. Despite the widespread use of shower simulation codes, there are relatively few formal reports in the literature specific to the comparison between experiment and simulations, especially in the range 1 GeV and above[9–11].

Accordingly, in this paper we present comparisons of some longitudinal and transverse shower distributions. Several materials and initial energies have been considered. Experimental results include data reported in 1969-1970, as well as a recent set, and they made use of quite different techniques. The simulations were made with EGS5[12], a recently released version of the EGS code system.

2 EGS5: An improved version of the EGS4 code system

The EGS code system, in both versions 3 and 4, was written in the language Mortran3 [13], which facilitated the introduction, by users, of new physics or algorithms in the form of Mortran macros. In this manner, over about 20 years, improvements and updates were incorporated into the distributed EGS4 code.

EGS5[12], released in December 2005, contains most of the bug-fixes and enhancements made to EGS4 since 1985. It also implements substantial additional improvements. For example, the electron transport mechanics has been completely revised. A dual random hinge approach [14], in which energy loss and multiple elastic scattering are fully decoupled, has been adopted for modeling the spatial transport of electrons and positrons. This preserves

near-second-order spatial moments of the transport equation over long step lengths and allows for transport across boundaries between regions of different media. In addition to providing an improved treatment of longitudinal and lateral displacement, the new charged track mechanics is expected to give an advantage in computational speed over models that use a boundary sensitive approach. The transport system should be adaptable easily to tracking codes that perform ray-tracing in combinatorial geometry without boundary sensitivity.

Other changes that are pertinent to results reported in this paper are:

• For electrons with energies in the range 1 keV to 100 MeV, an option is available for replacing the standard Molière model for multiple elastic scattering with a more exact one by Goudsmit and Saunderson[15].

• Options are available to turn on sampling of the angular distribution for Bremsstrahlung and pair production processes.

• ICRU-37 [16] collision and radiative stopping powers are used.

• Media data files, formerly prepared using PEGS4 (Preprocessor for EGS4) before the simulation study, are now automatically created at the inception of the EGS5 run.

• Mortran3, now an unsupported legacy code, has been replaced with Fortran, a change sufficient in itself to justify revalidation of the code.

3 Experimental measurements of electromagnetic showers

Most types of charged particle detectors have been used to observe electromagnetic cascade showers. The choice of detector depends on experimental needs, but not all would be suitable for wide range studies of shower profiles. Common disadvantages are limited range of linearity, perturbation of the shower by the detector itself and difficulty achieving adequate statistical weight. Two experiments performed in 1969-1970 [9,10], specifically to characterize electromagnetic showers in several materials, are particularly suitable for benchmarking because they measured deposited energy to large radii and depths. They used small detectors with good spatial resolution that perturbed the shower to a minimal extent, and controlled the beam in order to keep the detectors in a verifiably linear range. A recent paper [11] presented data from a systematically quite different, but well controlled, arrangement. A large planar detector was used behind various thicknesses of material, and although it did not report on the tails of the shower, it allows a test of simulations at

considerably higher incident energy.

From the published descriptions of these experiments, simulations have been made and compared with the quoted results. These comparisons will now be discussed in turn.

4 Showers at 1 GeV

4.1 Description of the experiment

Showers made in water and aluminum by 1 GeV electrons were discussed by Crannell and collaborators[9]. For water, the detector was a small crystal of anthracene ($C_{14}H_{10}$), selected to match the effective atomic number of water as closely as possible. The scintillation light was transmitted through an acrylic light pipe to a photomultiplier tube whose amplified signal was digitized. For the aluminum data, CaF_2 scintillator was selected. The beam intensity was measured, pulse-by-pulse, using a gas Cherenkov counter, and its energy was known to 0.5%.

In the $122 \times 122 \times 460\text{cm}^3$ water tank (3.4 radiation lengths transverse, 12.7 radiation lengths long), the detector could be positioned remotely along or transverse to the shower, and in this way a map of the shower density was made.

The aluminum experiment used $61 \times 61\text{cm}^2$ plates of various thicknesses, pressed together for a total thickness of 180 cm in the beam direction (6.9 radiation lengths transverse, 20.2 longitudinal). The specific gravity of the block was listed as 2.7, with no uncertainty given. In this experiment, the detector was placed in a deep well that was drilled in the mid-plane of one of the plates, and so could move only transversely. The beam was interrupted to allow this assembly to be repositioned for each new depth in the shower.

Each radial distribution was graphed and numerically integrated by the experimenters in order to produce a longitudinal distribution. Corrections were included for energy deposited beyond the technically restricted maximum radius of measurement. The area under this longitudinal plot was taken to represent the beam energy deposition. The experimental results in radius and depth were then reported in tables as percentages of the total energy deposition signal.

4.2 Comparison with water data

For the simulation of the water experiment, an EGS5 user code based on a cylinder-slab geometry was created. This was similar to the version uccyl.f in the EGS5 code distribution. The concentric cylindrical radii ranged from 1 cm to the outer radius of 68.8 cm, corresponding to the same cross sectional area as the water tank. Matching the experiment, the water slabs were 20 cm thick at the beginning of the shower, but increased in stages beyond shower maximum, as far as the full 460 cm. The 0.0015 radiation length beam window was ignored. The radiation length used for water was 36.09 cm.

In this, and all other simulations done for this paper, runs were made with various kinetic energy cutoffs for electrons and photons. It was found that using lower cutoffs than 100keV did not change the results within statistics, and so 100 keV was taken as a standard. Also, for all simulations reported here, the default multiple scattering option (Molière) was selected, as were the options to sample angular distributions for Bremsstrahlung and pair production. A parameter, `CHARD`, in the new transport system in EGS5 is used in selecting the optimal multiple scattering step size, and was set to 0.5 cm (see the User Manual Appendix B[12]).

The longitudinal profiles out to 10 radiation lengths are compared in Fig. 1. The statistical uncertainty on the EGS5 results (the hollow circles) are much smaller than the experimental uncertainties — as is the case for all results reported in this paper. The experimental uncertainties were stated to be ±3% in energy deposition, increasing to 10% by the end of the detector (12.7 radiation lengths), because of the extrapolation needed beyond the restricted range of the radial measurements. Uncertainty in the folding of the beam spot shape with the detector effective size increased the uncertainty in the first centimeters of the water to 30%. In our comparison, we make use of their average over the first 20 cm, and have assigned an uncertainty of ±10% to this bin. Additionally, the depth uncertainty was ±0.5 cm. Note that the two plots are not fitted to each other. There were no free parameters in the simulation. Fig. 2 shows the discrepancy between EGS5 and experiment, expressed as a ratio. Over most of the shower, the agreement is within 4%, with a possibly significant discrepancy ∼10% in the initial 40 cm.

As a model-independent and physically simple way of parameterizing the difference between simulation and data, we have used the mean depth of the energy deposition in the longitudinal shower profile. This was obtained numerically as $(\sum_1^n depth \times signal)/(\sum_1^n signal)$. The summation was over the range of bins in depth. Similarly, the width of the peak was parameterized as the RMS of the distribution about the mean depth. For water, the mean depth from the simulation is 0.7±0.8% shorter than that of the experiment.

The RMS width from the simulation is the same as that of the experiment with an uncertainty of ±0.8%. The uncertainties were estimated by simulating 200 shower profiles populated randomly according to the above experimental uncertainties, and measuring the fluctuations in the mean depth and width.

Longitudinal distributions broken down into radial shells are illustrated in Fig. 3. Aside from the discrepancy mentioned above the agreement is generally satisfactory in the peak of the shower. The simulation tends to report a signal ∼10% lower than experiment for radii 1 to 6 cm and depths above 200 cm.

4.3 Comparison with aluminum data

The case of aluminum was simulated in a similar way. It was assumed that the aluminum was pure, although this was not addressed by the original authors. Energy deposition was recorded in rings from 1 cm radius to 34.4 cm radius, and longitudinal slabs starting with 10 cm thicknesses, but increasing in thickness beyond a depth of 100 cm, out to the full 180 cm. The aluminum density was set at 2.7 gcm^{-3}, and the radiation length 8.894 cm. The value 0.5 was retained for the parameter `CHARD`.

The comparison may be seen out to about 13 radiation lengths in Fig. 4, and the ratio plot of Fig. 5. The experimental signal uncertainties were again ±3%, rising to ±10% by 180 cm depth. As above, for the beam shape effect, we assign an uncertainty of ±10% to the first 10 cm deep bin. The depth uncertainty was quoted to be (+0.32 -0.08) cm. It is evident that there is a systematic disagreement, with the simulation falling below the experimental results by as much as 20% at 12 radiation lengths. Much of this could be removed if the radiation length in the simulation were to be increased by about 4%, for example by assuming a lower density for the aluminum. This, however, seems to be well outside the measurement uncertainties stated in the paper. The densities we find listed for likely aluminum alloys fall in the range -1% to +3% about a nominal 2.7 gm cm^{-3}.

Evaluation of the mean depths shows the simulation to be 4.8±0.6% short of the experiment, and its RMS width also 3.3±0.8% narrower.

Distributions broken down into concentric rings are shown in Fig. 6. At radii above about 5 cm the experiment measured ∼10% higher energy deposition than calculated by EGS5.

5 Showers at 6 GeV

5.1 Description of the experiment

An investigation of shower energy deposition by 6 GeV electrons[10] was carried out using silver phosphate glass dosimeters, 1 mm diameter by 6 mm long. It was shown that relative errors in dose measurements between samples were less than 5%. The dosimeters were inserted in 1 mm diameter holes in a 6 mm thick plate of the metal to be studied. The total area of dosimeter holes was less than 0.5% of the plate area. This plate was installed with its long axis parallel to the beam direction, and pressed between blocks of the same material. Note that the dosimeters were transverse to the beam direction.

Materials studied were aluminum (with 3% magnesium) of $40 \times 40 \times 150\text{cm}^3$, copper of $40 \times 40 \times 56\text{cm}^3$ and lead (with 4% antimony) of $30 \times 30 \times 30\text{cm}^3$. This corresponded to 16.6, 38.9 and 51.7 radiation lengths long, respectively.

The beam spot was measured to be 10 mm by 6 mm FWHM, and this has been incorporated in the simulation. Different exposure times were used to cover 6 orders of magnitude in energy deposition density, and, to control the normalization, the beam was monitored with glass dosimeters and secondary emission monitors.

Results were presented on semi-logarithmic graphs. The sum of the signals in the steps in each graph was set to unity. For the comparisons made below, the graphs have been scanned and digitized. Longitudinal distributions for all three metals were given, with radial distributions from copper and lead. The 5% sample-to-sample uncertainty, referred to above, translates to uncertainties varying between 4% and 2% when the radial points are summed to obtain the longitudinal distributions.

5.2 Depth profile in aluminum

For the 6 GeV study, the EGS5 simulations used a similar user code to that discussed above. The `CHARD` multiple scattering step parameter was set to 0.125 cm, as was also the case for the copper and lead simulations described below. The experimenters did not give uncertainties for the densities of the metals. In this case, (97% Al - 3% Mg), they list a specific gravity of 2.66, which was used in the simulation with a radiation length of 9.04 cm. We find that industrial specifications for comparable alloys are in the range from 2.67 to 2.69. The longitudinal profiles are compared in Fig. 7. The plot of the ratio between simulation and experiment is in Fig. 8. In the case of aluminum,

the authors did not provide enough information to compute uncertainties in the longitudinal plots based on the 5% dosimeter errors. In the above two graphs we have applied uncertainties based on those calculated for the case of copper, a slight overestimate. For most of the depth range the agreement between simulation and experiment is within a few percent. At depths of 10 cm or shallower where there are 20% discrepancies, the experimental transverse sampling density, which seems to have been 5mm and comparable with the beam FWHM of 6 mm, may have been too coarse, leading to interpolation errors.

Comparing the mean depths of the experimental and simulated shower longitudinal profiles, it is found that the EGS5 shower depth is 2±0.3% longer than the experimental value (by comparison, it was 4.8±0.6% short of the experiment at 1 GeV). However, the EGS5 value for the RMS width of the profile peak is narrower than experiment, by 0.9±0.3% over the range 0 to 10 radiation lengths, and 0.6±0.3% over 0 to 15 radiation lengths (as against 3.3±0.8% narrower than experiment at 1 GeV). The depth discrepancy appears to be larger than the possible systematic uncertainty in the material.

5.3 Depth profile in copper

In the case of copper, the simulation used concentric rings from 0.125 cm out to 23 cm, with longitudinal slabs corresponding to the spacing in the experiment. The simulation of the heavier elements made use of photon splitting for large depths. This is a fluctuation reduction technique, and was implemented by finding each gamma ray appearing beyond a depth of 30 cm, copying it 30 times, and using a weight of 1/30 for each copy. The experimenters quote a radiation length of 1.44 cm and a specific gravity of 8.9. Industrial listings of specific gravity for wrought copper are 8.89 to 8.96, although for cast copper it may be 8.69. The simulation used the same radiation length, 1.44 cm, corresponding to a specific gravity of 8.93.

The two graphs of the longitudinal profile in copper are in Fig. 9 and in Fig. 10. The ratio plot shows a large discrepancy at small depths, as if 0.5 cm of copper were missing from the front of the simulation. Alternatively, the experimental transverse sampling density may again have been too coarse at shallow depths, and led to interpolation errors. Beyond 20 cm (14 radiation lengths), the simulation falls steadily below the measurement, the ratio reaching 50% at 52 cm (36 radiation lengths).

The mean depths of the shower profiles, evaluated in the range 0 to 12 radiation lengths, are 4.7±0.4% longer for EGS5 than for the experiment. The discrepancy in the deep tails of the distribution reduces this difference to 4.1%

beyond 30 radiation lengths. Again the simulation has a slightly narrower peak than the data. The RMS width is 2.4±0.4% narrower when evaluated over 0 to 12 radiation lengths, and 1.8% narrower over 0 to 18 radiation lengths. The difference between simulation and experiment is not understood.

5.4 Depth profile in lead

In the case of lead, the experimental results were originally plotted using a value for the radiation length, 0.532 cm, for (96% Pb - 4% Sb), that was lower than the accepted value (0.58 cm). This was done by the experimenters (for this one graph only) to facilitate comparison with an earlier shower calculation[17]. We have used their 0.532 to transform the depth values to centimeters. For this lead-antimony alloy the specific gravity is given by the experimenters as 11.1, and listed in tables of alloys as 11.04. In the simulation, the value 11.1 was used, the radiation length being 0.580 cm.

The geometry was set up in rings starting at 0.125 cm and extending to 17 cm, with longitudinal slabs to match the experiment. The longitudinal plots for lead, Fig. 11 and Fig. 12, once again indicate a small systematic shift between experiment and model. And again the yield from the simulation falls below the measurement deep in the shower. The difference increases to 30% at 20 cm (34 radiation lengths), deep in the tail of the shower. The fluctuations in the tail of the ratio plot, Fig. 12, originate in the experimental data: the simulation profile has statistics high enough that it is quite smooth.

Unlike the cases of aluminum and copper, for lead the mean depth calculated for the EGS5 simulation is shorter than experimentally observed. The difference increases as greater depths are included. It is 1.1±0.3% evaluated up to 12 radiation lengths, increasing to 3.5±0.3% for 24 radiation lengths. However, the simulation RMS widths are once again narrower than experiment, by 1.5±0.3% and 3.8±0.3% over the ranges up to 12 and 24 radiation lengths respectively. In this case the RMS width difference seems to scale with the discrepancy in mean depth. The discrepancy again appears to be outside the likely range of uncertainties in the material.

As a summary of the 6 GeV results of the shower cores, the mean depth differences between EGS5 and experiment for Al, Cu and Pb respectively, are 2±0.3%, 4.7±0.4% and -1.1±0.3%. For the widths the values are -0.9±0.3%, -2.4±0.4% and -1.5±0.3%.

5.5 Lateral distribution in copper

The experimenters presented profiles of the transverse spread of energy deposition at depths of 5, 15 and 20 radiation lengths in copper, obtained from the off-axis dosimeters. In comparing these with EGS5 simulations, the graphs have again been normalized to equal areas. The comparison may be seen in Fig. 13. At shallow depths, the simulation appears to show a central peak perhaps 25% wider than the experiment, at the contour where intensity has dropped to 10% of the peak.

5.6 Lateral distribution in lead

Transverse distributions for lead were reported at depths of 5, 12 and 24 radiation lengths. The comparison with simulation is illustrated in Fig. 14. Again, at shallow depths the simulation of the central peak is slightly wider than experiment, in this case by about 10% at the point where the intensity has dropped to 10% of the peak. Very deep in the lateral tails, beyond 8 cm, the EGS5 density falls below experiment by a factor of $\sim$2.

6 Showers at 28.5 GeV

6.1 Description of the experiment

An experiment has been reported[11] that examined the longitudinal profile of showers generated by an electron beam at 28.5 GeV. The shower material, ceramic bricks of alumina, Al_2O_3, with a 10% admixture of silica, SiO_2, was stacked in boxes, one behind the other, along the line of the beam. The nominal box thicknesses, from upstream to downstream, were 4, 4, 4, and 2 radiation lengths, and a detector was positioned after the last box. The boxes could be moved on to or off the beam line under remote control. In this way, thicknesses of nominally 2, 6, 10 and 14 radiation lengths could be selected with minimal air gaps front of the detector. The shower material immediately in front of the detector had transverse dimensions equivalent to 7 radiation lengths. Behind the detector, the shower was allowed to disperse in the radiation enclosure. Results from intermediate thicknesses of 4, 8, and 10 radiation lengths were also recorded. In these cases, however, because of space constraints, the box immediately in front of the detector, 2 radiation lengths thick, could not be fully withdrawn from the spreading shower, leaving a partially occluded 15 cm air gap in front of the detector. The uncertainty in the mean density

measured for the material was about 0.1%, while the thicknesses of the boxes were measured to better than ±0.5% for the thinnest unit and 0.25% for the others.

The detector was a helium filled, parallel-plate ion chamber with eleven thin gaps. Care was taken over linearity in both the ion chamber signal pulse and the toroid used to measure the beam pulse intensity.

6.2 Shower depth profiles in alumina

A summary of results was presented as a plot of the various signals at the available thicknesses, normalized so that the sum of all the entries was set to unity. The data at 4, 8 and 12 radiation lengths were included, despite the small shift caused by the partial gap in the shower material. By repeating data-collection runs in different sequences, the effect of drift in sensitivity was minimized, and uncertainties at each thickness setting could be estimated from the observed fluctuations.

In the original publication, shower simulations were made using the earlier code release, EGS4, with a user code based on a rectangular geometry, more appropriate for the experiment than the cylinder-slab geometry employed in the lower energy simulations above. For the purpose of efficient computation, the radiation length thickness of each box, including the thin aluminum walls, was calculated, and represented by the equivalent thickness of pure alumina. The box thickness in cm was modeled exactly as measured by adjusting the alumina density in the input data file. Because of the very low energy deposition in the helium of the ion chamber, the energy deposit in the body of the chamber was used as a surrogate, since the helium signal would scale in proportion with it. The ion chamber was then modeled as an aluminum plate of low density.

For the present work, the various geometries have been simulated in EGS5, with a user code, ucxyz.f for rectangular geometry, making use of the same structures as for the original publication (see the Appendix). The modeled signals were plotted in the same way as the reported data. The energy cutoffs in the vicinity of the simulated detector were 10 keV, but 100 keV elsewhere for efficiency. The `CHARD` parameter was 0.1 cm.

The simulated and experimental profiles are shown in Fig. 15, and the ratio between them at each thickness entry is in Fig. 16. The mean depth calculation used above gives a difference of $0.34 \pm 0.14\%$ between EGS5 and the experiment, with a difference in the widths of the peaks of $0.12 \pm 0.14\%$. This level of agreement indicates that EGS5 gives an accurate representation of most of the shower profile at 28.5 GeV, at least for material of relatively low atomic

number. Unlike the studies at lower energy, however, neither the longitudinal nor transverse deep tails of the shower profile were studied.

7 Effects not simulated and summary

The EGS5 code incorporates a detailed treatment of the $e^{\pm}$ and γ interactions with the medium. Some processes that are not treated in our simulation are muon-pair production, the LPM effect [18], and photonuclear interactions with subsequent neutron scattering. The muon pair production rate is suppressed by $\sim 2.4 \times 10^{-5}$ relative to the electron processes in showers, but most of the muons penetrate deeply, and their collective energy deposit profile roughly corresponds to the integral over depth of the electron shower profile. However, even as deep as the point where the shower profile has fallen to 1% of its peak, the muons provide less than 1% of that signal. The LPM effect in showers becomes significant in the multi-TeV range. Neither of these processes is expected to affect the observations reported here, but in some experimental conditions their effects cannot be ignored.

The photo-neutron production cross section peaks in the giant dipole resonance region of gamma ray energies, 10-20 MeV, yielding neutrons in the few MeV range. The fraction of the shower energy in neutrons is $\sim 10^{-3}$[19], and the shower's evolving photon spectrum is more favorable, by a factor of $\sim$2, to neutron production later in the shower than at the peak. Neutrons disperse roughly isotropically from their point of origin, typically losing energy in sequential scatters. Their material-dependent attenuation length is somewhat shorter than the radiation length in the case of hydrogenous material, but longer for material of high atomic number. This effect contributes little to longitudinal or transverse broadening of the shower until the main electromagnetic component has become attenuated by a factor of >100.

In summary, electromagnetic shower profiles in materials ranging from water to lead have been compared with simulations using EGS5. There is general agreement to within a few percent in the region of shower maximum, and near the radial core. Discrepancies in the range of tens of percent, and even as great as 50%, have been encountered, however, at depths beyond about twice the depth of shower maximum, and these increase with depth.

In order to help understand the processes involved, and improve the simulations, it would be helpful to have access to further, systematically well studied, experimental data. A wider range in beam energy would be helpful, with good coverage in depth and radius, and, of course, materials with a wide range of atomic number.

8 Acknowledgments

We wish to thank Drs H. Hirayama, Y. Namito, A. Bielajew and S. Wilderman, authors (with W.R.N.) of the EGS5 code, and Dr. K. Tesch for helpful comments.

References

[1] R.L. Ford and W.R. Nelson, The EGS Code System: Computer programs for the Monte Carlo simulation of electromagnetic cascade showers (Version 3), Stanford Linear Accelerator report SLAC-210 (1978); W.R. Nelson, H. Hirayama and D.W.O. Rogers, The EGS4 Code System, Stanford Linear Acelerator Center report SLAC-265 (1985); for a recent development, extensively used at low energies, see I. Kawrakow and D.W.O. Rogers, The EGSnrc Code System: Monte Carlo Simulation of Electron and Photon Transport, National Research Council of Canada, PIRS-701, (Nov. 2003).

[2] P.A. Aarnio et al., International Conference on Monte Carlo Simulation in High Energy and Nuclear Physics, MC93, p 100, World Scientific, Singapore, 1994.

[3] Geant4 collaboration, Nucl. Instr. and Meth. A506 (2003) 250.

[4] R. Brun et al., Proc. 2nd International Conference on Calorimetry in High Energy Physics, p. 82, World Scientific, Singapore, 1992.

[5] R.E. Prael and H. Lichtenstein, User Guide to LCS: The LAHET Code System, Los Alamos National Laboratory report LA-UR-89-3014 (1989)

[6] H. Fesefeldt, Simulation of hadronic showers, physics and application, RWTH Aachen Physics Institute report PITHA 85/02 (1985).

[7] T.A. Gabriel, J.E. Brau and B.L. Bishop, The physics of compensating calorimetry and the new CALOR89 Code System, Oak Ridge National Laboratory report ORNL/TM-11060 (1989).

[8] P. Cloth, D. Filges, R.D. Neef and G. Stertzenbach, HERMES, a Monte Carlo program system for beam-materials interaction studies, Forschungszentrum Jülich GmbH report KFA/JUL-2203, code package NEA-1265/02 (1988).

[9] C.J. Crannell, H. Crannell, R.R. Whitney and H.D. Zeman, Phys Rev. 184 (1969) 426.

[10] G. Bathow et al., Nucl. Physics B20 (1970) 592.

[11] J. Belz et al., Astroparticle Physics 25 (2006) 57

[12] H. Hirayama et al., The EGS5 Code System, Stanford Linear Accelerator Center report SLAC-R-730 (2005).

[13] A.J. Cook, Mortran3 Users Guide, Stanford Linear Accelerator Center Computation Research Group Technical Memorandum CGTM-209 (1983);

[14] A.F. Bielajew and S.J. Wilderman, Proceedings of the 2nd International Workshop on EGS4, High Energy Accelerator Research Organization (KEK) report Proceedings 2000-20 (2000), p1.

[15] S. Goudsmit and J.L. Saunderson, Phys. Rev. 57 (1940) 24.

[16] Stopping powers for electrons and positrons: International Commission on Radiation Units and Measurements, Bethesda, Md., ICRU Report 37, 1984.

[17] U. Völkel, DESY reports 65/6 (1965) and 67/16 (1967).

[18] L.D. Landau and I.J. Pomeranchuk, Dokl. Akad. Nauk. SSSR 92 (1953) 535, 735; A.B. Migdal, Phys. Rev. 103 (1956) 1811.

[19] H. DeStaebler, T.M. Jenkins and W.R. Nelson, The Stanford Two Mile Accelerator Project, Ed. R.B. Neal, Benjamin, N.Y. (1968) Chapter 26.

Appendix

The following is an example of the geometry data file to be read in by a getxyz subroutine in a ucxyz user code package from the EGS5 archive. Details of the various parameters will be found in the code listing. This example is for the nominal 4 radiation length geometry. Here the first two alumina boxes are out of the beam and replaced by air. The fourth box occupies part of its nominal on-beam volume, the rest being replaced by air. Text on the right of each line is commentary.

```
ucxyz-flash: 4 rl.data
         5                      NMED (I10)
AL2O3                           MEDIA(J,1) (24A1)
AL                              MEDIA(J,2) (24A1)
AIR0p1MeV                       MEDIA(J,3)
Ion chamber                     MEDIA(J,4)
FLASH chamber                   MEDIA(J,5)
       0.1       0.1            ECUTin,PCUTin (Kinetic) (MeV) (2F10.0)
        10         9        15 IMAX,JMAX,KMAX (3I10)
     -26.5                      XBOUND(cm), (F10.0) no 4 block
   -26.353                      effective bound of no 3 block
    -21.44                      eff bound no 2 block
   -16.028                      eff bound no 1 block
     -4.25                      air scint. box beam aperture offset
      2.65
      4.60                      measured beam offset Jul 15 2005
    16.028
     21.44
```

```
 26.353
   26.5
  -26.5                    YBOUND,(cm), (F10.0)
-26.353
 -21.44
-16.028
  -1.85                    Offset beam windows
   5.05
 16.028
  21.44
 26.353
   26.5
  -0.16                    ZBOUNDS (CM) end of vacuum
    0.0                    end of beam window (AL)
  32.21                    back of 1st AL2O3 block
 32.5275                   back of  gap
 64.7375                   back of 2nd AL2O3 block
 64.9915                   back of air gap 1/2 way thr block 3
 97.2015                   back of 3rd Al2O3 block
 97.6790                   back of air gap
114.5065                   back of final Al2O3 block
115.1415                   back of Al plate
121.1415                   back of FLASH air gap
121.7765                   back of AL plate
124.2765                   2.5 cm gap to ion chamber
125.3830                     back face 3/8 Al plate+glue+inactive plate
128.2130                   back face of ion chamber core
129.1870                   back face of back AL plate
  5    5    5    5    1    1    2       0.0 1/16 in vac window
  4    7    4    6    2    2    3       0.0 air instead of no 1
  3    8    3    7    4    4    3       0.0 air instead of no 2
  2    9    2    8    6    6    1      3.49 AL2O3 no 3 effective
  1    6    1    9    8    8    3       0.0 AIR half of blk4
  7   10    1    9    8    8    1    3.4767 Al2O3 no 4 effective
  1   10    1    4    9    9    2       0.0 Al face of air scint. box
  1   10    6    9    9    9    2       0.0 with beam hole
  1    4    5    5    9    9    2       0.0 approxd. as
  6   10    5    5    9    9    2       0.0 square
  1   10    1    9   10   10    5       0.0 AIR in scint chamber
  1   10    1    4   11   11    2       0.0 Al back face of air scint.
  1   10    6    9   11   11    2       0.0 box with beam hole
  1    4    5    5   11   11    2       0.0 approxd. as
  6   10    5    5   11   11    2       0.0 square
  1   10    1    9   13   13    2       0.0 3/8 Al wall+inactive plate
  1   10    1    9   14   14    4     1.397  ION CHAMBER (aluminum)
```

```
  1   10    1    9   15   15    2       0.0 3/8 Al back wall
                                             blank card (required EOF)
   -0.05      0.05           XLOWER,XUPPER(cm) (2F10.0)
   -0.05      0.05           YLOWER,YUPPER(cm) (2F10.0)
   -0.16         1           N.B. Zin(cm) ,Kin (F10.0,I10)
     0.0       0.0       1.0 Uin,Vin,Win (3F10.0)
       1         4           luxlev,inseed (2I10)
  6      1000                nbatches (I5),ncases (I10)
 28500.0        -1         0 ekein(Mev),iqin,isamp (F10.0,2I10)
  0    0    0                ipeangsw,iedgesw,iraysw (3I5)
  0    0    0    0           ipolarsw,incohrsw,iprofrsw,impacrsw (4I5)
  1    2    0    0           ibrdst,iprdst,ibrspl,nbrspl (4I5)
     0.1                     chard(1) (cm) (F10.0)
```

The following example is for the nominal 14 radiation length configuration, with all alumina boxes in place on the beam line.

```
ucxyz-flash: 14 rl.data (AE=AP=10 keV, ecut=pcut=10 keV k.gt.9)
         5                   NMED (I10)
AL2O3                        MEDIA(J,1) (24A1)
AL                           MEDIA(J,2) (24A1)
AIR0p1MeV                    MEDIA(J,3)
Ion chamber                  MEDIA(J,4)
FLASH chamber                MEDIA(J,5)
       0.1       0.1         ECUTin,PCUTin (Kinetic) (MeV) (2F10.0)
         9         9        15 IMAX,JMAX,KMAX (3I10)
     -26.5                   XBOUND(cm), (F10.0) no 4 block
   -26.353                   effective bound of no 3 block
    -21.44                   eff bound no 2 block
   -16.028                   eff bound no 1 block
     -4.25                   offset air scint. box beam aperture
      2.65
     16.028
     21.44
     26.353
      26.5
     -26.5                   YBOUND,(cm), (F10.0)
   -26.353
    -21.44
   -16.028
     -1.85                   offset beam windows
      5.05
     16.028
     21.44
     26.353
```

```
   26.5
  -0.16                    ZBOUNDS (CM) end of vacuum
    0.0                    end of beam window (AL)
  32.21                    back of 1st AL2O3 block
 32.5275                   back of  gap
 64.7375                   back of 2nd AL2O3 block
 64.9915                   back of air gap
 97.2015                   back of 3rd Al2O3 block
 97.6790                   back of air gap
114.5065                   back of final Al2O3 block
115.1415                   back of Al plate
121.1415                   back of FLASH air gap
121.7765‘                  back of AL plate
124.2765                   2.5 cm gap to ion chamber
125.3830                     back of Al plate,glue,inactive plate
128.2130                   back face of ion chamber core
129.1870                   back face of back AL plate,glue
  5    5    5    5    1    1    2       0.0 1/16 in vac window
  4    6    4    6    2    2    1      3.49 AL2O3 no 1 effective
  3    7    3    7    4    4    1      3.49 AL2O3 no 2 effective
  2    8    2    8    6    6    1      3.49 AL2O3 no 3 effective
  1    9    1    9    8    8    1    3.4767 Al2O3 no 4 effective
  1    9    1    4    9    9    2       0.0 Al face of air scint box
  1    9    6    9    9    9    2       0.0 with beam hole
  1    4    5    5    9    9    2       0.0 approxd. as
  6    9    5    5    9    9    2       0.0 square
  1    9    1    9   10   10    5       0.0 AIR - scint. chamber
  1    9    1    4   11   11    2       0.0 Al back face of pizza
  1    9    6    9   11   11    2       0.0 box with beam hole
  1    4    5    5   11   11    2       0.0 approxd. as
  6    9    5    5   11   11    2       0.0 square
  1    9    1    9   13   13    2       0.0 3/8 Al wall
  1    9    1    9   14   14    4     1.397 ion ch as Al
  1    9    1    9   15   15    2       0.0 3/8 Al back wall
                                          blank card (required EOF)
  -0.05      0.05           XLOWER,XUPPER(cm) (2F10.0)
  -0.05      0.05           YLOWER,YUPPER(cm) (2F10.0)
  -0.16         1           N.B. Zin(cm) ,Kin (F10.0,I10)
    0.0       0.0       1.0 Uin,Vin,Win (3F10.0)
      1        14           luxlev,inseed (2I10)
  6      1000                nbatches (I5),ncases (I10)
28500.0        -1         0 ekein(mev),iqin,isamp (F10.0,2I10)
  0    0    0                ipeangsw,iedgesw,iraysw (3I5)
  0    0    0    0           ipolarsw,incohrsw,iprofrsw,impacrsw (4I5)
  1    2    0    0           ibrdst,iprdst,ibrspl,nbrspl (4I5)
```

```
0.1                     chard(1) (cm) (F10.0)
```

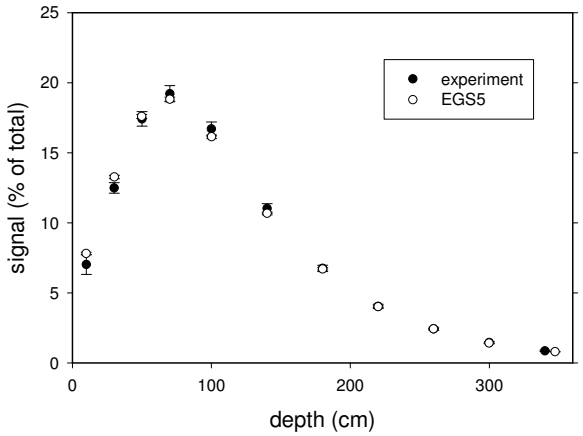

Fig. 1. Experimental and simulated longitudinal shower profiles of 1 GeV electrons in water.

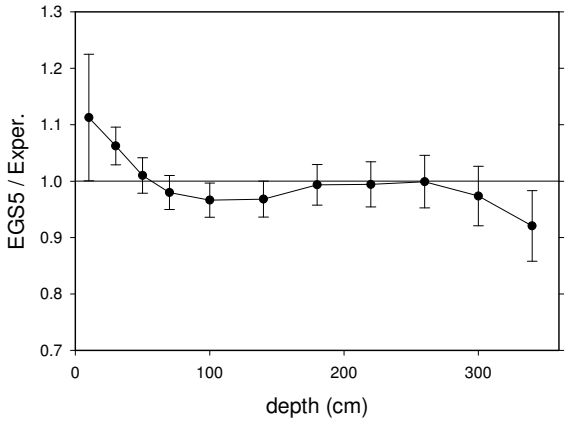

Fig. 2. Ratio between simulation and experimental intensities from the longitudinal shower profile of 1 GeV electrons in water.

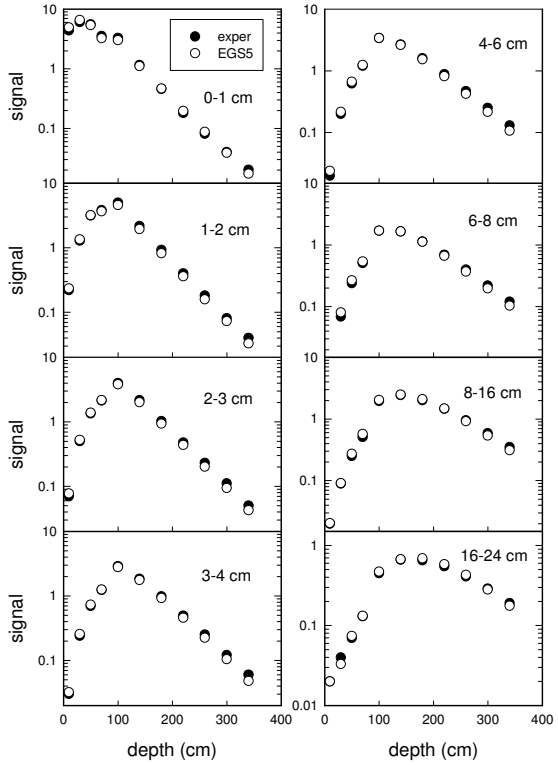

Fig. 3. Shower longitudinal energy deposition profiles of 1 GeV electrons in water, broken down into radial shells.

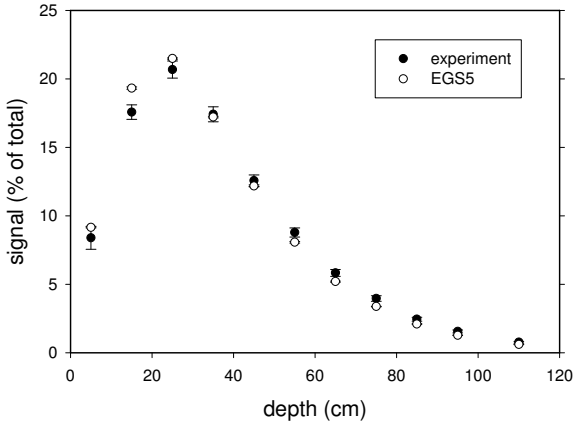

Fig. 4. Experimental and simulated longitudinal shower profiles of 1 GeV electrons in aluminum.

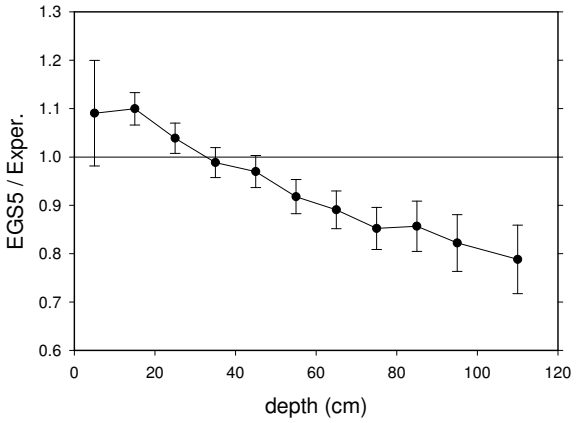

Fig. 5. Ratio between simulation and experimental intensities from the longitudinal shower profile of 1 GeV electrons in aluminum.

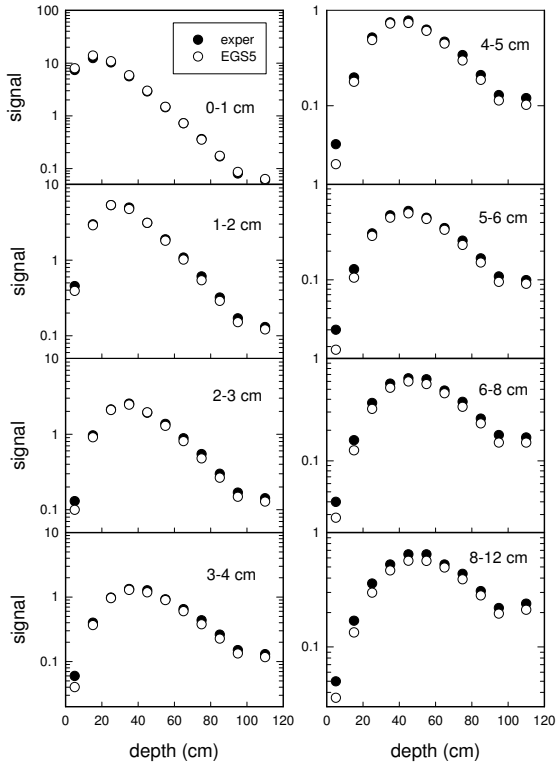

Fig. 6. Shower longitudinal energy deposition profiles of 1 GeV electrons in aluminum, broken down into radial shells.

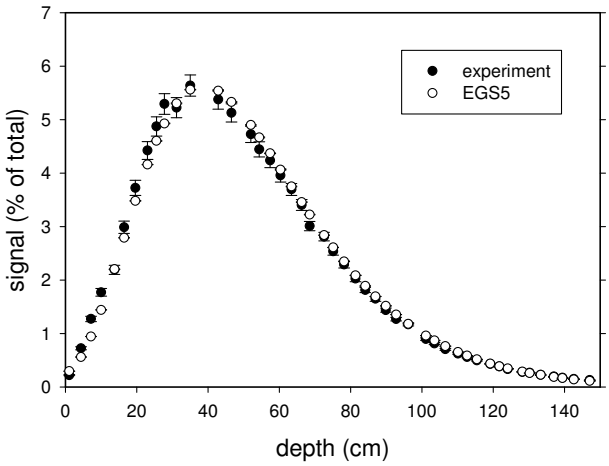

Fig. 7. Experimental and simulated longitudinal shower profiles of 6 GeV electrons in aluminum.

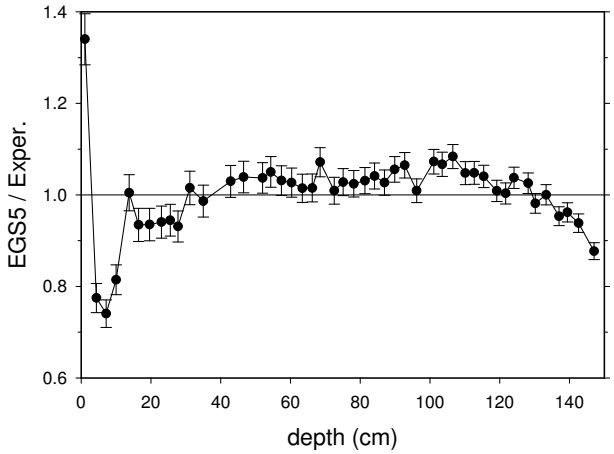

Fig. 8. Ratio between simulation and experimental intensities from the longitudinal shower profile of 6 GeV electrons in aluminum.

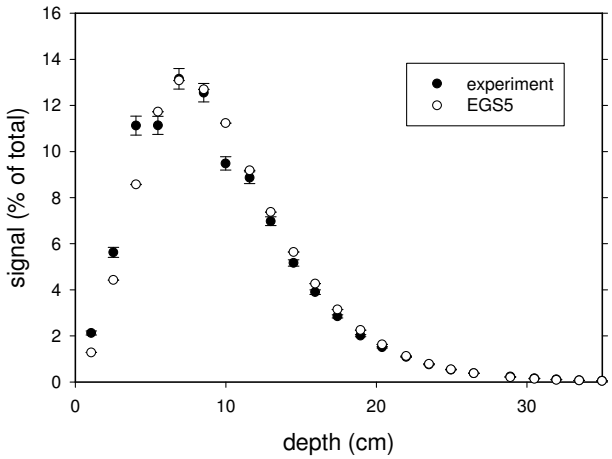

Fig. 9. Experimental and simulated longitudinal shower profiles of 6 GeV electrons in copper.

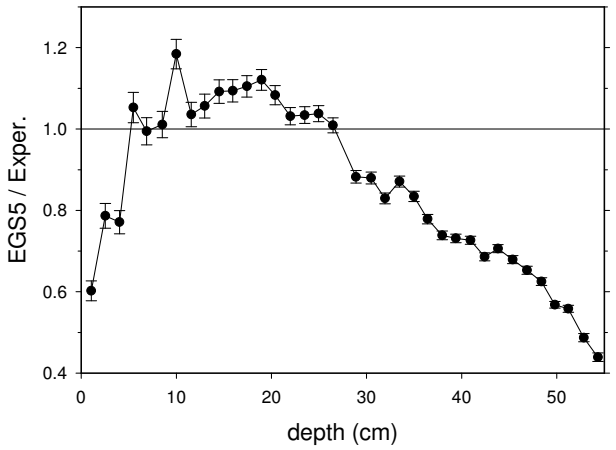

Fig. 10. Ratio between simulation and experimental intensities from the longitudinal shower profile of 6 GeV electrons in copper.

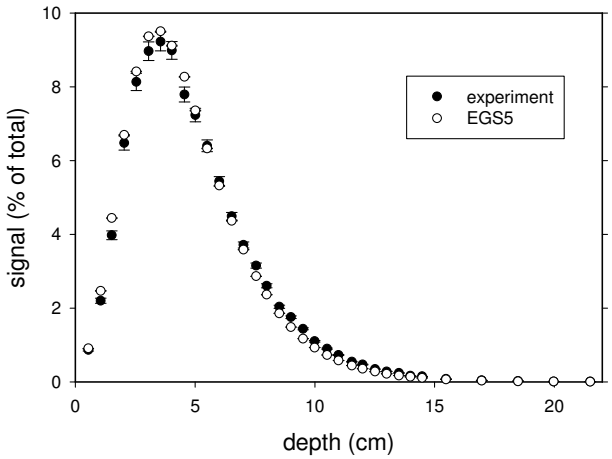

Fig. 11. Experimental and simulated longitudinal shower profiles of 6 GeV electrons in lead.

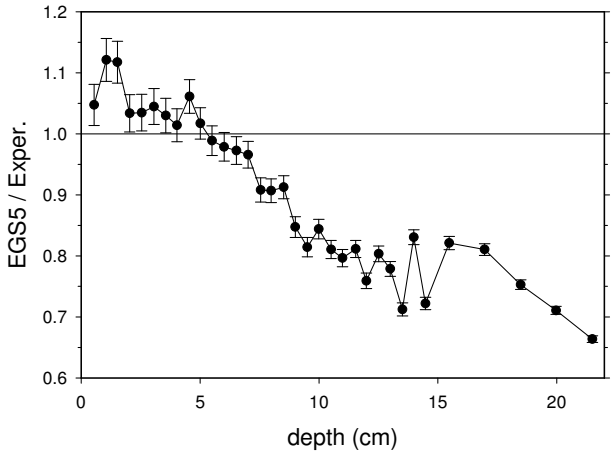

Fig. 12. Ratio between EGS5 simulation and experimental intensities from the longitudinal shower profile of 6 GeV electrons in lead.

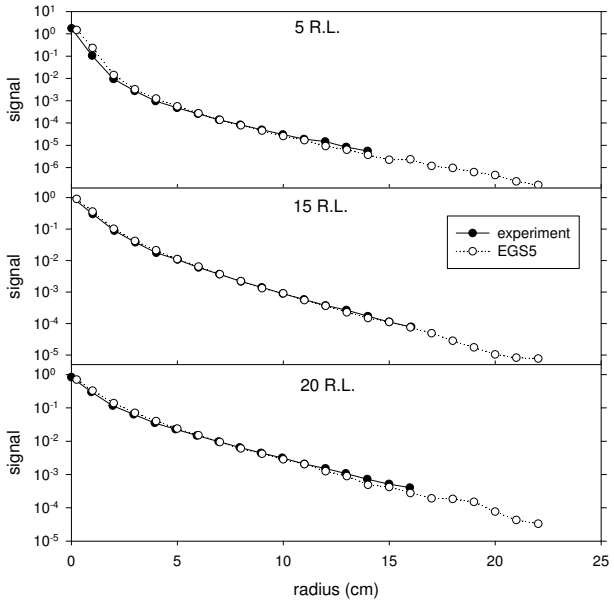

Fig. 13. Lateral distributions of the 6 GeV shower in copper at various depths.

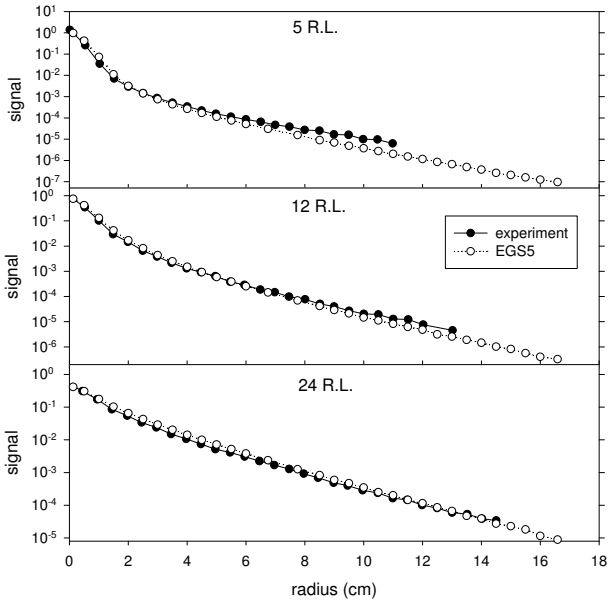

Fig. 14. Lateral distributions of the 6 GeV shower in lead at various depths.

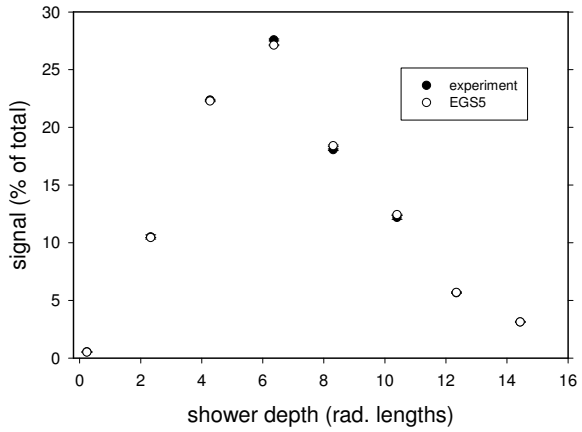

Fig. 15. Shower signals at 28.5 GeV detected behind alumina of various thicknesses. EGS5 and experimental signals are separately normalized so that their sums equal unity.

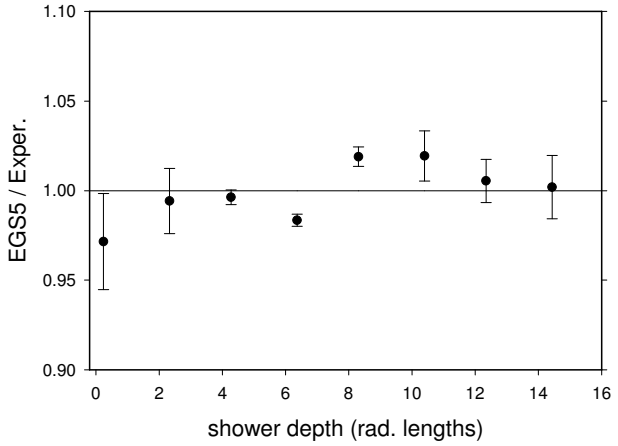

Fig. 16. Ratio of EGS5 to experimental normalized signals behind alumina of various thicknesses (28.5 GeV).